Journal of Electrochemistry

Volume 25 | Issue 6

2019-12-28

Ionic Liquid Assisted Synthesis of Porous Carbons from Rice Husk for Supercapacitors

Han-fang ZHANG

Feng WEI

Jian SUN

Meng-ying JING

Xiao-jun HE
School of Chemistry and Chemical Engineering, Anhui Key Lab of Coal Clean Conversion and Utilization, Anhui University of Technology, Maanshan 243002, China;, agdxjhe@126.com

DOI: 10.13208/j.electrochem.180721 **Artical ID**:1006-3471(2019)06-0764-09
Cite this: *J. Electrochem.* **2019**, *25*(6): 764-772 **Http**://electrochem.xmu.edu.cn

Ionic Liquid Assisted Synthesis of Porous Carbons from Rice Husk for Supercapacitors

ZHANG Han-fang, WEI Feng, SUN Jian, JING Meng-ying, HE Xiao-jun*
(*School of Chemistry and Chemical Engineering, Anhui Key Lab of Coal Clean Conversion and Utilization, Anhui University of Technology, Maanshan* 243002, *China*)

Abstract: It is still a challenge to prepare carbon materials with high specific surface area at low cost from renewable resources. Herein, the authors report an efficient approach to synthesize porous carbons (PCs) from rice husk with ionic liquid (1-butyl-3-methylimidazolium hexafluorophosphate ($BMIMPF_6$)) as a template and an activation agent. The as-made PCs featured the high specific surface area up to 1438 $m^2 \cdot g^{-1}$. As electrodes for supercapacitors, PCs showed a high specific capacitance of 256 $F \cdot g^{-1}$ at 0.05 $A \cdot g^{-1}$ in 6 $mol \cdot L^{-1}$ KOH aqueous electrolyte and a good rate performance of 211 $F \cdot g^{-1}$ at 10 $A \cdot g^{-1}$. All the PC electrodes exhibited good cycle stability. This work provides a new way for efficient synthesis of PCs from biomass using $BMIMPF_6$ as a template and an assisted activation agent for high-performance supercapacitors.

Key words: porous carbon; $BMIMPF_6$; rice husk; supercapacitor
CLC Number: O646 **Document Code:** A

With the fast consumption of fossil fuel and the following global environmental concerns, there is an increasing demand for green, sustainable, and highly efficient energy-storage devices. Supercapacitors have drawn much attention as the promising energy storage devices in recent years because of their high power density and long cycle life[1-2]. Among the components of supercapacitor, electrode materials play an important role in supercapacitive performance [3]. There are various electrode materials, including porous carbons (PCs), transition metal oxides or sulfides, conducting polymers and so on[4-9]. Among these electrode materials, PCs are indispensable candidates due to their high surface area, chemical stability and electrical conductivity[10]. Up to now, the experiment conditions[11-13] influence the pore structure parameters and the cost of PCs. It is imperative to develop a simple and effective procedure for the synthesis of PCs from cheap carbon sources for the commercial applications of supercapacitors. The non-renewable and limited fossil sources including coal[14], coal tar pitch[15] and petroleum coke[16], have been used to synthesize PCs. Compared to the fossil sources, the use of renewable carbon sources to produce PCs is worthwhile and necessary from the view point of economic, environmental and social issues. Rice husk is usually treated as waste and disposed at power plant sites, which leads to a serious environmental problem[17]. Therefore, it is necessary to make full use of rice husk. Rice husk is one of the promising precursors for the production of low-cost PCs since the annual outputs of rice husk in the world and China are huge, which are up to 148 and 40 million tons, respectively[18]. However, the high ash content in rice husk makes it difficult to be utilized because the deash procedure increases its cost, which leads to the large discard of rice husk.

Ionic liquids (ILs) have been extensively studied because IL inherits many excellent features, such as good solubility for chemicals, excellent thermal stability and negligibly small vapor pressure[19-21]. IL (1-butyl-3-methylimidazolium hexafluorophosphate,

Received: 2018-07-21, Revised: 2018-12-04 *Corresponding author, Tel: (86-555)2311807, E-mail: agdxjhe@126.com

($BMIMPF_6$)) has been used as a template to synthesize carbon xerogels from resorcinol-formaldehyde by coupling with KOH activation for supercapacitors[21]. Nevertheless, no study on the synthesis of PCs from rice husk using $BMIMPF_6$ as a template for supercapacitor has been reported. $BMIMPF_6$ is expects to work both as template for the formation of pores and activation agent to tune the pores via the HF formed *in-situ*.

Herein, we report a facile method to prepare PCs from rice husk using $BMIMPF_6$ as a template and an assisted activation agent. The effects of $BMIMPF_6$/rice husk mass ratio on the pore structure parameters and electrochemical performance of PCs in 6 mol·L^{-1} KOH aqueous electrolyte for supercapacitors are addressed in details.

1 Experimental

1.1 Materials

The rice husk was obtained from Huai-xiang Company in Anhui province, as described elsewhere[12]. Carbon black was provided by Cabot Co., USA. The $BMIMPF_6$ was purchased from Shanghai Flute Cypress Chemical Technology Co. Ltd. of China. Other chemicals were purchased from Aladdin Co. Ltd.

1.2 Syntheses

For a typical run, $BMIMPF_6$ was added into 150 mL absolute ethanol. The deash rice husk was added into the above mixture and dispersed by ultrasonic for 1 h, followed by being soaked under vacuum for 3 h. Then, the resultant mixture was dried at 80 ℃ for 3 h to obtain the reactant. The reactant was transferred to a corundum boat that was put in a box-type electric furnace and heated at 3 ℃·min^{-1} to 330 ℃ for 30 min, and then heated to 750 ℃ in a flowing N_2 atmosphere (60 mL·min^{-1}). The resultant product was washed with 2 mol·L^{-1} HCl solution and distilled water to remove the inorganic impurities, and dried at 110 ℃ for 24 h before use. The obtained PC is denoted as $PC_{x/y}$, where the subscript x/y represents the mass ratio of $BMIMPF_6$/rice husk. In addition, the deash rice husk prepared without $BMIMPF_6$ is denoted as RHC.

1.3 Characterizations

The pore structure of PCs was studied by N_2 adsorption-desorption technique at -196 ℃ using ASAP2010. The BET surface area (S_{BET}) of PCs was calculated by the BET (Brunauer-Emmett-Teller) equation in a relative pressure range from 0.05 to 0.24. The pore size distribution was calculated by the density functional theory (DFT) method. The total pore volume (V_t) was obtained at a relative pressure of 0.99, and the micropore volume (V_{mic}) was estimated by using the t-plot method. The average pore size (D_{ap}) of PCs was obtained by the equation of $D_{ap} = 4V_t/S_{BET}$. The microstructures of PCs were investigated by X-ray diffraction (XRD, Philips X, Cu *K*, Radiation) and transmission electron microscope (TEM, JEOL-2100). The thermal stability of $BMIMPF_6$ was studied by heating $BMIMPF_6$ at 800 ℃ in flowing nitrogen of 30 mL·min^{-1} in a thermogravimetric analyzer (DTG-60, Japan).

1.4 Electrochemical Measurements

The carbon electrodes were made by mixing PC (87wt%), carbon black with BET surface area of 550 $m^2·g^{-1}$ (5wt%) and polytetrafluoroethylene (8wt%), and then pressed at 20.0 MPa for 10 s, followed by being dried at 110 ℃ for 1 h under vacuum. Button-type supercapacitor was assembled with two similar carbon electrodes (about 11 mg·cm^{-2}) separated by a polypropylene membrane in 6 mol·L^{-1} KOH electrolyte. The supercapacitor was evaluated by cyclic voltammetry on a CHI760C electrochemical workstation (CH Instrument, Shanghai, China). The charge-discharge performance of supercapacitor was carried out on a supercapacitance test system (SCTs, Arbin Instruments, USA). The specific capacitance of PC electrode (C, F·g^{-1}) was calculated from the slope of the discharge curve according to Eq. (1).

$$C = \frac{2I}{m\frac{\Delta V}{\Delta t}} \tag{1}$$

where I is the discharge current (A), ΔV is the discharge voltage between the Δt period, and m is the mass (g) of the active materials in a single electrode.

The energy density (E, Wh·kg^{-1}) and average power density (P, W·kg^{-1}) of supercapacitors were

calculated according to Eqs. (2) and (3).

$$E = \frac{1}{2 \times 4 \times 3.6} CV^2 \quad (2)$$

$$P = \frac{E}{\Delta_{td}} \quad (3)$$

where C is the capacitance of two-electrode supercapacitor (F), and V is the usable voltage after IR drop (V), and Δ_{td} is the discharge time (h).

The gravimetric capacitance of PC electrodes (C, F·g^{-1}) was also calculated from the CV curves according to Eq. (4).

$$C = \frac{2\int_{V_1}^{V_2} i(V)dV}{mv\Delta V} \quad (4)$$

where V_1 and V_2 (V) are the lower and upper limits of potential, respectively; $\Delta V = V_2 - V_1$, is the voltage window; v is the scan rate (V·s^{-1}); and i (V) is the current as the function of voltage.

The electrochemical impedance spectroscopic (EIS) measurements were performed on a CHI760C electrochemical workstation (CH Instrument, Shanghai, China). The specific capacitance of PC electrodes was also obtained by Eq. (5).

$$C = -\frac{4}{2\pi mfZ''} \quad (5)$$

where f is the frequency (Hz) and Z'' is the imaginary impedance (Ohm).

The surface area normalized capacitance C_{sa} (μF·cm^{-2}) was calculated by Eq. (6).

$$C_{sa} = \frac{C}{S_{BET}} \times 100 \quad (6)$$

where S_{BET} is the specific surface area (m^2·g^{-1}) of PC derived from the N_2 adsorption and C is the specific capacitance of the single electrode (F·g^{-1}).

2 Results and Discussion

Fig. 1(A) shows the N_2 adsorption-desorption isotherms of PCs. Fig. 1(B) is the corresponding pore size distribution curves of PCs. All the PCs synthesized in the present work are microporous carbons, evidenced by the Type I isotherms in accordance with the IUPAC classification. The pore size distribution curves of PCs revealed that the micropores of PCs centered at 0.7 nm, 1.0 nm, 1.2 nm and 2.0 nm. The pore structure parameters of PCs are shown in Tab. 1. The S_{BET} of $PC_{3/1}$ reached 1438 m^2·g^{-1}. The S_{mic}, V_{mic}, S_{BET} and V_t values of PCs rose with the increase of $BMIMPF_6$/rice husk mass ratio, which is mainly ascribed to the highest content of $BMIMPF_6$ template as well as the *in-situ* activation agent of HF produced from the decomposition of $BMIMPF_6$, as shown in Eq. (7). The S_{BET} of PCs decreased from 1438 m^2·g^{-1} ($PC_{3/1}$) to 697 m^2·g^{-1} ($PC_{1/2}$) when the mass ratio of $BMIMPF_6$/rice husk dropped from 3/1 to 1/2 with other conditions remaining unchanged. Obviously, the S_{BET} of PCs can be tuned by adjusting the mass ratio of $BMIMPF_6$ to rice husk. It was reported that the S_{BET} of hierarchical PCs synthesized through the self-assembly of poly(benzoxazine-co-resol) with ionic liquid $C_{16}mimBF_4$ both as a structure directing agent and a heteroatom precursor reached 596 m^2·g^{-1}[19]. The S_{BET} of carbon xerogels synthesized from resorcinol-formaldehyde with ionic liquid BMImCl as a template reached 590 m^2·g^{-1}[20]. The S_{BET} of carbon xerogels

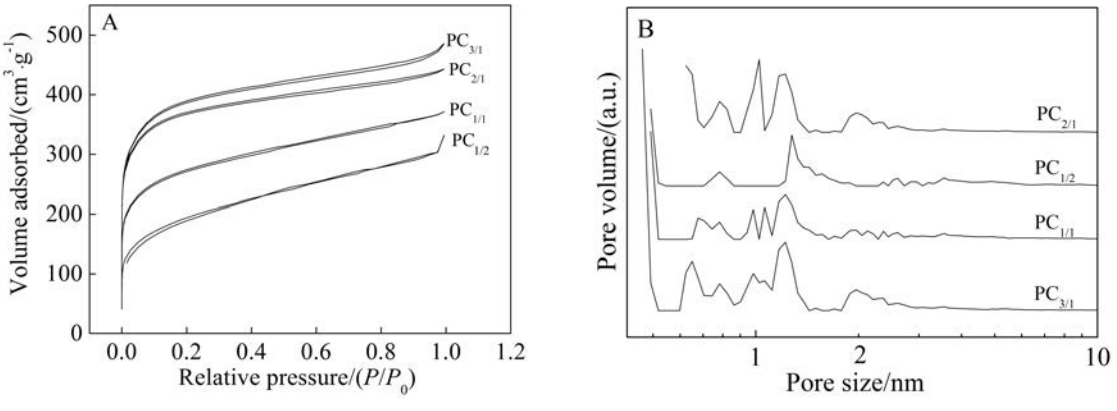

Fig. 1 (A) Nitrogen adsorption-desorption isotherms and (B) pore size distribution curves of PCs.

Tab. 1 Pore structure parameters of PCs

PCs	D_{ap}/nm	S_{BET}/($m^2 \cdot g^{-1}$)	S_{mic}/($m^2 \cdot g^{-1}$)	V_{mic}/($cm^3 \cdot g^{-1}$)	V_t/($cm^3 \cdot g^{-1}$)	V_{mic}/V_t/%
$PC_{1/2}$	2.95	697	369	0.16	0.51	31.3
$PC_{1/1}$	2.33	988	696	0.29	0.58	50.0
$PC_{2/1}$	1.99	1375	1165	0.48	0.69	69.6
$PC_{3/1}$	2.09	1438	1203	0.50	0.75	66.7

synthesized from resorcinol-formaldehyde without coupling with KOH activation reached 667 $m^2 \cdot g^{-1}$[21]. The above results show that $BMIMPF_6$ is a good template for the synthesis of PCs from rice husk via the *in-situ* activation of HF produced from the decomposition of $BMIMPF_6$.

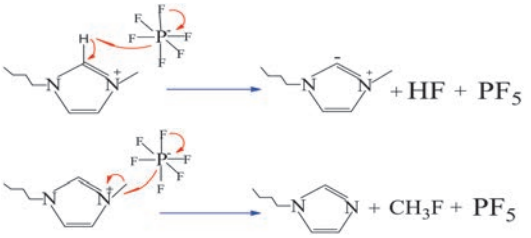

Fig. 2 shows the TEM images of $PC_{2/1}$ and $PC_{3/1}$. As shown in Fig. 2(A) and (B), the mesopores (ca. 5 nm) and a few macropores can be observed in thin $PC_{2/1}$. In addition, many carbon dots (ca. 5 nm in diameter) can be found in $PC_{2/1}$, which might be formed via the *in-situ* activation of HF produced from the decomposition of $BMIMPF_6$ on the surface of carbon materials as shown in Fig. 2(C) and (D). For the $PC_{3/1}$, abundant carbon dots are also observed in Fig. 2(E) and (F), and the diameter of the carbon dots is ca. 10 nm. The sheet-like structure of $PC_{2/1}$ can be demonstrated by FESEM images in Fig. S1(A) and (B) (Supporting Information). The FESEM images of RHC are also provided in Fig. S1 (E) and (F) (Supporting Information), showing large bulk morphology. Compared with $PC_{2/1}$, $PC_{3/1}$ possesses thinner sheets (Fig. S1 (C) and (D), Supporting Information), resulting from the increased dosage of $BMIMPF_6$. The porous carbon sheets with abundant carbon dots are expected to improve the capacitance and rate performance as supercapacitor electrode[22].

Fig. 3(A) is the thermogravimetric curve of $BMIMPF_6$ in nitrogen atmosphere. As we all know,

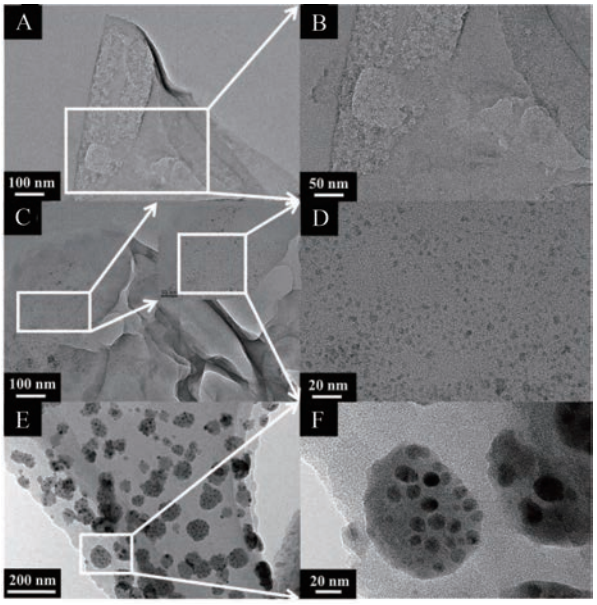

Fig. 2 (A) TEM image of $PC_{2/1}$; (B) high-resolution TEM image of $PC_{2/1}$; (C) TEM image of $PC_{2/1}$, the inset is the high-resolution TEM image; (D) high-resolution TEM image of the inset in Fig. 2(C); (E) TEM image of $PC_{3/1}$; (F) high-resolution TEM image of $PC_{3/1}$.

$BMIMPF_6$ is an organic salt that exists as a liquid below a threshold temperature (ca. 100 ℃), which can be used as green solvents due to its negligible vapor pressure, non-flammability and high thermostability. Fig. 3(A) shows that $BMIMPF_6$ began to be decomposed at ca. 340.2 ℃ and ended at ca. 398.6 ℃. During the heating process, liquid $BMIMPF_6$ firstly entered the microstructures of rice husk and acted as a template at lower temperature. Secondly, at higher temperature, $BMIMPF_6$ was decomposed into a 1-butyl-3-methylimidazolium carbene, HF and PF_5 via Eq. (7) or a 1-butylimidazole, methyl fluoride and PF_5 via Eq. (8)[23]. Lastly, the HF formed *in-situ* works as an activation agent to make abundant pores by

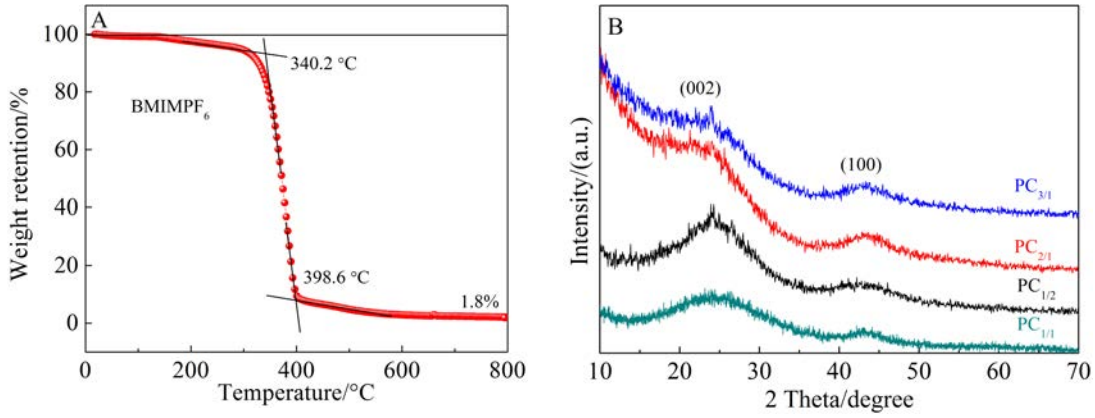

Fig. 3 (A) Thermogravimetric curve of $BMIMPF_6$ in nitrogen atmosphere. (B) XRD patterns of PCs.

reacting with the carbon precursor produced from rice husk. Fig. 3(B) is the XRD patterns of the PCs with no sharp peaks being observed, indicative of the amorphous structure of PCs due to the activation effect of HF formed *in-situ* from the decomposition of $BMIMPF_6$.

Fig. 4(A) shows that the galvanostatic charge-discharge curves of PC electrodes in 6 mol·L^{-1} KOH electrolyte at 0.8 A·g^{-1} are symmetrical without obvious pseudocapacitance behavior, and the *IR* drop of $PC_{3/1}$ was only 0.028 V. Fig. 4(B) is the specific capacitance of PC electrodes in 6 mol·L^{-1} KOH electrolyte at different discharge current densities. The specific capacitances of $PC_{3/1}$ and $PC_{2/1}$ reached 256 F·g^{-1} (17.8 μF·cm^{-2}) and 260 F·g^{-1} (18.9 μF·cm^{-2}) at 0.05 A·g^{-1}, respectively. In addition, the specific capacitance of RHC was only 103 F·g^{-1} at 0.05 A·g^{-1} (Fig. S2(A), Supporting Information). At 0.05 A·g^{-1}, the specific capacitance of $PC_{2/1}$ became the highest among four samples, which is attributed to the abundant carbon dots in the $PC_{2/1}$. With the increase of current density to 10 A·g^{-1}, the specific capacitance of $PC_{3/1}$ was 211 F·g^{-1} with a capacitance retention of 82.4%, exhibiting a superior rate performance.

Fig. 4(C) shows the cycle stability of PC electrodes. The specific capacitance of $PC_{3/1}$ electrode remained 245 F·g^{-1} after 1000 charge-discharge cycles at 0.1 A·g^{-1}. It is interesting to note that the capacitance of $PC_{3/1}$ electrodes increased slightly in the first 500 cycles and remained 104.3% of the initial capacitance after 10000 cycles. The rise of the specific capacitance may be due to the improvement of wettability, which indicates good electrochemical stability and reversibility of the PC electrodes. In order to find out the advantages of $PC_{3/1}$ synthesized in this work, we compared the specific surface area, specific capacitance, and stability of $PC_{3/1}$ with those reported in literatures. As listed in Tab. S1, $PC_{3/1}$ possessed high capacitance and excellent cycle stability in 6 mol·L^{-1} KOH electrolyte. In our previous work, the specific capacitance of PCs synthesized from rice husk by $ZnCl_2$ activation remained 243 F·g^{-1} at 0.05 A·g^{-1} after 1000 cycles[24]. It was reported that the specific capacitance of carbon xerogels synthesized from resorcinol-formaldehyde without coupling with KOH activation was below 150 F·g^{-1} at different current densities[21]. The specific capacitance of carbon nanocages made from benzene reached 178 F·g^{-1} at 10 A·g^{-1} in 6 mol·L^{-1} KOH electrolyte[25]. It should be beared in mind that rice husk, the carbon source of PCs in our present work, is much cheaper than benzene. For nitrogen-rich networks, the specific capacitance reached 173 F·g^{-1} at 10 A·g^{-1}[26]. For functionalized 3D hierarchical PC, the specific capacitance reached 192 F·g^{-1} at 10 A·g^{-1} in 6 mol·L^{-1} KOH electrolyte[27]. For porous graphene made with flake-like MgO as a template and ferrocene as the carbon precursor, the specific capacitance was 196 F·g^{-1} at 10 A·g^{-1}[28]. Obviously, $PC_{3/1}$ with high specific capacitance and good cycle stability in our present work is very attractive as the electrode of supercapacitors. For $PC_{3/1}$ synthesized in our present work, its volumetric capacitance reach-

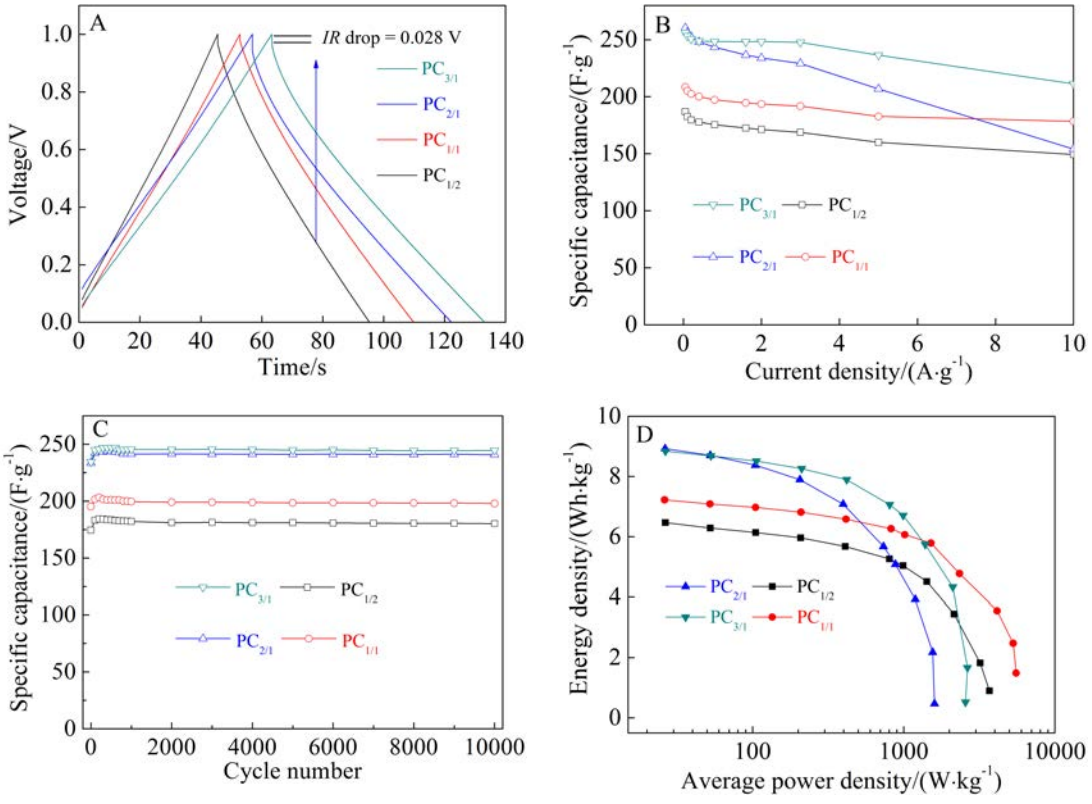

Fig. 4 (A) Charge-discharge curves of PC electrodes in 6 mol·L^{-1} KOH electrolyte at 0.8 A·g^{-1}; (B) specific capacitance plots of PC electrodes at different discharge current densities; (C) capacitance variation of PC electrodes at 0.1 A·g^{-1}; (D) Ragone plots of PC supercapacitors.

es 129 F·cm^{-3} at 0.8 A·g^{-1} in 6 mol·L^{-1} KOH electrolyte, which is based on that the bulk density of $PC_{3/1}$ is 0.52 g·cm^{-3}. It was reported that the volumetric capacitance of ionic liquid $C_{16}mimBF_4$ assisted synthesis of poly(benzoxazine-co-resol)-based hierarchically porous carbons was 101 F·cm^{-3} at 0.5 A·g^{-1} in 6 mol·L^{-1} KOH electrolyte[19]. The volumetric capacitances of the MOF-derived nanoporous carbons in 6 mol·L^{-1} KOH electrolyte ranged from 81 to 165 F·cm^{-3}[29]. Fig. 4(D) shows the Ragone plots of PC supercapacitors. The energy densities of $PC_{2/1}$ capacitor and $PC_{3/1}$ capacitor were 8.93 Wh·kg^{-1} and 8.84 Wh·kg^{-1} at 0.05 A·g^{-1}, respectively.

Fig. 5(A) is the CV curves of PC electrodes at a scan rate of 2 mV·s^{-1}. All the samples exhibited the symmetric rectangular shapes. With the scan rate increasing to 100 mV·s^{-1}, the CV curves still remained the symmetric rectangular shapes, demonstrating good rate capability and ideal electrical double layer behavior (Fig. 5(B)). The specific capacitances of $PC_{3/1}$ and $PC_{2/1}$ electrodes calculated from the CV curves at 2 mV·s^{-1} reached 239 F·g^{-1} (16.6 μF·cm^{-2}) and 247 F·g^{-1} (17.9 μF·cm^{-2}), respectively, while 142 F·g^{-1} (9.8 μF·cm^{-2}) and 138 F·g^{-1} (10.0 μF·cm^{-2}) at 100 mV·s^{-1}, respectively. In addition, the CV curves of RHC electrodes at scan rates of 2 to 100 mV·s^{-1} are provided in Fig. S2(B) (Supporting Information). The RHC electrodes also showed a rectangular shape. As shown in Fig. 5(C), the short x-intercept (0.62 Ohm) of $PC_{3/1}$ electrode reveals that the $PC_{3/1}$ electrode had low contact resistance and material resistance. The diameter of the semicircle of PC electrodes is smaller than that of RHC electrodes at low frequency, indicating that PC electrodes had smaller charge-discharge resistance (the inset in Fig. 5(C) and Fig. S2(C)) (Supporting Information). Fig. 5(D) is the specific capacitance of PC electrodes at different frequencies. The maximum capacitance occurred at the lowest fre-

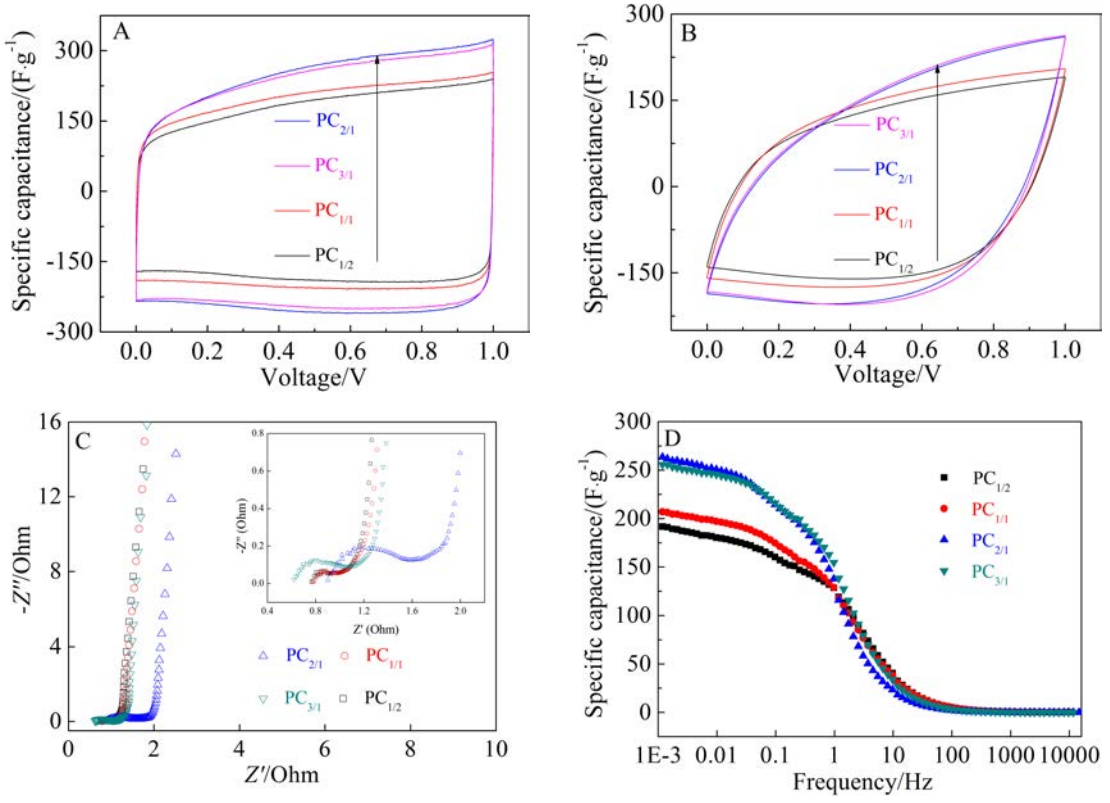

Fig. 5 (A) CV curves of PC electrodes at 2 mV·s^{-1}; (B) CV curves of PC electrodes at 100 mV·s^{-1}; (C) Nyquist plots of PC electrodes; (D) specific capacitance plots of PC electrodes at different frequencies.

quency of 0.001 Hz, showing a value of 264 F·g^{-1} (19.2 μF·cm^{-2}) for $PC_{2/1}$ and 256 F·g^{-1} (17.8 μF·cm^{-2}) for $PC_{3/1}$. At 1.0 Hz, the capacitance of $PC_{2/1}$ remained 129 F·g^{-1}, while 138 F·g^{-1} for $PC_{3/1}$. It was reported that the capacitance of PCs made from direct coal liquefaction residue and cetyltrimethylammonium bromide was ca. 150 F·g^{-1} at 1.0 Hz in 6 mol·L^{-1} KOH electrolyte[30].

3 Conclusions

PCs were made from rice husk with $BMIMPF_6$ as a template and an assisted activation agent. The results show that the pore sizes of PCs centered at 0.7, 1.0, 1.2 and 2.0 nm. With the increased mass ratio of $BMIMPF_6$/rice husk from 1/2 to 3/1, the specific surface area of PCs rose from 697 m^2·g^{-1} to 1438 m^2·g^{-1}. PC electrodes show a high specific capacitance of 256 F·g^{-1} at 0.05 A·g^{-1} in 6 mol·L^{-1} KOH aqueous electrolyte, a good rate performance of 211 F·g^{-1} at 10 A·g^{-1} and a superior cycle stability with the retention of 104.3% initial capacitance after 1000 cycles. This work paves a new way for efficient synthesis of PCs from biomass sources using $BMIMPF_6$ as a template and an assisted activation agent for high-performance supercapacitors.

Acknowledgements

This work was supported by the National Natural Science Foundation of China (Nos. U1508201, U1710116), the Provincial Innovative Group for Processing & Clean Utilization of Coal Resource.

Supporting Information Available

The supporting information is available free of charge via the internet at http://electrochem.xmu.edu.cn.

References:

[1] Jayaramulu K, Dubal D P, Nagar B, et al. Ultrathin hierarchical porous carbon nanosheets for high-performance supercapacitors and redox electrolyte energy storage[J]. Advanced Materials, 2018, 30(15): 1705789.

[2] Wang H Y, Zhou Q Q, Yao B W, et al. Suppressing the self-discharge of supercapacitors by modifying separators

with an ionic polyelectrolyte[J]. Advanced Material Interfaces, 2018, 5(10): 1701547.

[3] Lang J W(郎俊伟), Zhang X(张旭), Wang R T(王儒涛), et al. Strategies to enhance energy density for supercapacitors[J]. Journal of Electrochemistry(电化学), 2017, 23(5): 507-532.

[4] Huang T(黄涛), Tao G Z(陶广智), Yang C Q(杨重庆), et al. Template induced fabrication of nitrogen doped carbon sheets as electrode materials in supercapacitors[J]. Journal of Electrochemistry(电化学), 2017, 23(6): 604-609.

[5] Ye J L(叶江林), Zhu Y W(朱彦武). Porous carbon materials produced by KOH activation for supercapacitor electrodes[J]. Journal of Electrochemistry(电化学), 2017, 23 (5): 548-559.

[6] Zhou Y S(周岳珅), Li M(李梦), Wu S(吴双), et al. Morphology control of $ZnCo_2O_4$ electrode materials and their electrochemical properties study on supercapacitors [J]. Journal of Electrochemistry(电化学), 2019, DOI: 10.13208/j.electrochem.180625.

[7] Shen L F, Che Q, Li H S, et al. Mesoporous $NiCo_2O_4$ nanowire arrays grown on carbon textiles as binder-free flexible electrodes for energy storage[J]. Advanced Functional Materials, 2014, 24(18): 2630-2637.

[8] Ma L B, Hu Y, Chen R P, et al. Self-assembled ultrathin $NiCo_2S_4$ nanoflakes grown on Ni foam as high-performance flexible electrodes for hydrogen evolution reaction in alkaline solution[J]. Nano Energy, 2016, 24: 139-147.

[9] Su L, Gao L J, Du Q H, et al. Construction of $NiCo_2O_4$@MnO_2 nanosheet arrays for high-performance supercapacitor: Highly cross-linked porous heterostructure and worthy electrochemical double-layer capacitance contribution [J]. Journal of Alloys and Compounds, 2018, 749: 900-908.

[10] Zhang S, Sui L N, Kang H Q, et al. High performance of N-doped graphene with bubble-like textures for supercapacitors[J]. Small, 2017, 14: UNSP1702570.

[11] Yu D F, Chen C, Zhao G Y, et al. Biowaste-derived hierarchical porous carbon nanosheets for ultrahigh power density supercapacitors[J]. ChemSusChem, 2018, 11(10): 1678-1685.

[12] He X J, Ling P H, Qiu J S, et al. Efficient preparation of biomass-based mesoporous carbons for supercapacitors with both high energy density and high power density[J]. Journal of Power Sources, 2013, 240: 109-113.

[13] Chen C, Yu D F, Zhao G Y, et al. Three-dimensional scaffolding framework of porous carbon nanosheets derived from plant wastes for high-performance supercapacitors[J]. Nano Energy, 2016, 27: 377-389.

[14] Song X L, Guo J X, Guo M X, et al. Freestanding needle-like polyaniline-coal based carbon nanofibers composites for flexible supercapacitor [J]. Electrochimica Acta, 2016, 206: 337-345.

[15] He X J, Li X J, Ma H, et al. ZnO template strategy for the synthesis of 3D interconnected graphene nanocapsules from coal tar pitch as supercapacitor electrode materials [J]. Journal of Power Sources, 2017, 340: 183-191.

[16] Pan L, Wang Y X, Hu H, et al. 3D self-assembly synthesis of hierarchical porous carbon from petroleum asphalt for supercapacitors[J]. Carbon, 2018, 134: 345-353.

[17] Liu D C, Zhang W L, Lin H B, et al. A green technology for the preparation of high capacitance rice husk-based activated carbon[J]. Journal of Cleaner Production, 2016, 112: 1190-1198.

[18] Wu J Q, Yu D X, Zeng X P, et al. Ash formation and fouling during combustion of rice husk and its blends with a high alkali Xinjiang coal[J]. Energy & Fuels, 2018, 32(1): 416-424.

[19] Guo D C, Mi J, Hao G P, et al. Ionic liquid $C_{16}mimBF_4$ assisted synthesis of poly (benzoxazine-co-resol)-based hierarchically porous carbons with superior performance in supercapacitors[J]. Energy & Environmental Science, 2013, 6(2): 652-659.

[20] Yang H M, Cui X J, Deng Y Q, et al. Ionic liquid templated preparation of carbon aerogels based on resorcinol-formaldehyde: properties and catalytic performance [J]. Journal of Materials Chemistry, 2012, 22(41): 21852-21856.

[21] Wang G, Ling Z, Li C P, et al. Ionic liquid as template to synthesize carbon xerogels by coupling with KOH activation for supercapacitors[J]. Electrochemistry Community, 2013, 31: 31-34.

[22] Prasath A, Athika M, Duraisamy E, et al. Carbon-quantum-dot-derived nanostructured MnO_2 and its symmetrical supercapacitor performances[J]. ChemistrySelect, 2018, 3 (30): 8713-8723.

[23] Kroon M C, Buijs W, Peters C J, et al. Quantum chemical aided prediction of the thermal decomposition mechanisms and temperatures of ionic liquids[J]. Thermochimica Acta, 2007, 465(1/2): 40-47.

[24] He X J, Ling P H, Yu M X, et al. Rice husk-derived porous carbons with high capacitance by $ZnCl_2$ activation for supercapacitors [J]. Electrochimica Acta, 2013,105: 635-641.

[25] Xie K, Qin X T, Wang X Z, et al. Carbon nanocages as supercapacitor electrode materials[J]. Advanced Materials, 2012, 24(3): 347-352.

[26] Hao L, Luo B, Li X L, et al. Terephthalonitrile-derived nitrogen-rich networks for high performance supercapac-

itors[J]. Energy & Environmental Science, 2012, 5(12): 9747-9751.

[27] Qie L, Chen W M, Xu H H, et al. Synthesis of functionalized 3D hierarchical porous carbon for high-performance supercapacitors[J]. Energy & Environmental Science, 2013, 6(8): 2497-2504.

[28] Wang H J, Sun X X, Liu Z H, et al. Creation of nanopores on graphene planes with MgO template for preparing high-performance supercapacitor electrodes[J]. Nanoscale, 2014, 6(12): 6577-6584.

[29] Chaikittisilp W, Ariga K, Yamauchi Y. A new family of carbon materials: synthesis of MOF-derived nanoporous carbons and their promising applications[J]. Journal of Materials Chemistry A, 2013, 1(1): 14-19.

[30] Zhang J B, Jin L J, Cheng J, et al. Hierarchical porous carbons prepared from direct coal liquefaction residue and coal for supercapacitor electrodes[J]. Carbon, 2013, 55: 221-232.

离子液体辅助条件下由稻壳合成超级电容器用多孔炭

张韩方,魏 风,孙 健,荆梦莹,何孝军*

(安徽工业大学化学与化工学院,安徽省煤清洁转化与综合利用重点实验室,安徽 马鞍山 243002)

摘要: 本文以稻壳为碳源,以离子液体 1-丁基-3-甲基咪唑六氟磷酸盐($BMIMPF_6$)为模板和辅助活化剂制备了多孔炭材料(PCs). 多孔炭的比表面积达 1438 $m^2\cdot g^{-1}$,总孔容达 0.75 $cm^3\cdot g^{-1}$. 以 PCs 为超级电容器电极材料,6 $mol\cdot L^{-1}$ 的 KOH 溶液为电解液组装成扣式电池,在 0.05 $A\cdot g^{-1}$ 的电流密度下,比电容高达 256 $F\cdot g^{-1}$;当电流密度增大至 10 $A\cdot g^{-1}$,其比电容仍保持在 211 $F\cdot g^{-1}$,展现出好的倍率性能. 所得的多孔炭电极均表现出优异的循环稳定性. 这一工作以 $BMIMPF_6$ 作为模板和辅助活化剂,为合成生物质基超级电容器用多孔炭提供了一种新方法.

关键词: 多孔炭;1-丁基-3-甲基咪唑六氟磷酸盐离子液体;稻壳;超级电容器